# Closed-loop quantum interferometry for phase-resolved Rydberg-atom field sensing

Samuel Berweger,[1,*] Alexandra B. Artusio-Glimpse,[1] Andrew P. Rotunno,[1] Nikunjkumar Prajapati,[1] Joseph D. Christesen,[2] Kaitlin R. Moore,[3] Matthew T. Simons,[1] and Christopher L. Holloway[1]

[1] *National Institute of Standards and Technology, Boulder, Colorado 80305, USA*
[2] *SRI International, Boulder, Colorado 80302, USA*
[3] *SRI International, Princeton, New Jersey 08540, USA*

(Received 23 February 2023; revised 14 June 2023; accepted 25 September 2023; published 3 November 2023)

Although Rydberg-atom-based electric field sensing provides key advantages over traditional antenna-based detection, it remains limited by the need for a local oscillator (LO) for low-field and phase-resolved detection. In this work, we demonstrate that closed-loop quantum interferometric schemes can be used to generate a system-internal reference that can directly replace an external LO for Rydberg field sensing. We reveal that this quantum interferometrically defined internal reference phase and frequency can be used analogously to a traditional LO for atom-based down-mixing to an intermediate frequency for lock-in phase detection. We demonstrate that this LO-equivalent functionality provides analogous benefits to an LO, including full 360° phase resolution as well as improved sensitivity. The general applicability of this approach is confirmed by demodulating a four-phase-state signal broadcast on the atoms. Our approach may open up new sensing schemes and although the present implementation still uses an auxiliary rf field, we provide a clear path toward all-optical Rydberg-atom sensing implementations by discussing several schemes that allow for all-optical rf phase detection without the need for an external rf LO field.

DOI: 10.1103/PhysRevApplied.20.054009

## I. INTRODUCTION

Rydberg-atom-based field sensing is an emerging technology that uses resonant transitions between excited states at high principal quantum numbers, $n$, to detect radio-frequency (rf) electric ($E$) fields [1–3]. This technology has the potential to replace traditional wavelength-scaling antenna architectures with compact atomic vapor cells [4] that use an optical readout of the atomic response. However, similar to traditional rf-demodulation schemes, phase-sensitive detection often requires a local reference field. For the case of Rydberg atoms, an additional local-oscillator (LO) field can be applied, which will be mixed to an intermediate frequency (IF) by the atoms themselves (the "Rydberg mixer") [5,6]. This Rydberg mixer provides benefits including improved sensitivity [6,7], frequency selectivity [8,9], and phase sensitivity [10] that allow angle-of-arrival [11] detection and demodulation of phase-modulated communication signals [12]. However, a Rydberg mixer nevertheless requires an additional LO rf field radiating the atoms with a frequency within a few megahertz of the measured field and a matched phase front, which can be difficult to achieve and is undesirable in many applications.

One possible way to eliminate the need for an externally applied LO is to use a closed-loop scheme [13,14]. These schemes exploit the quantum mechanical interference across a set of driven transitions between discrete states that form a closed loop. These can be used to mutually reference the phases of fields across large frequency ranges [15]. Any transition between states in this loop will simultaneously occur in both directions, where interference between the two paths results in a transition probability that depends on the relative phases of all fields involved [16]. Such approaches have typically been applied to atomic ground-state transitions [15] but, more recently, Rydberg-atom loop schemes have emerged as an attractive means for phase transfer between optical and microwave photons for quantum communications applications [17,18]. Closed-loop schemes can be complex because of orbital-angular-momentum selection rules that require at least four transitions and in this respect a proposed scheme for Rydberg sensing that requires four rf fields is impractical [14]. A recent experimental implementation that drives two degenerate rf transitions succeeded at eliminating the need for additional rf fields, but was unable to achieve the full 360° phase

*sam.berweger@gmail.com

 

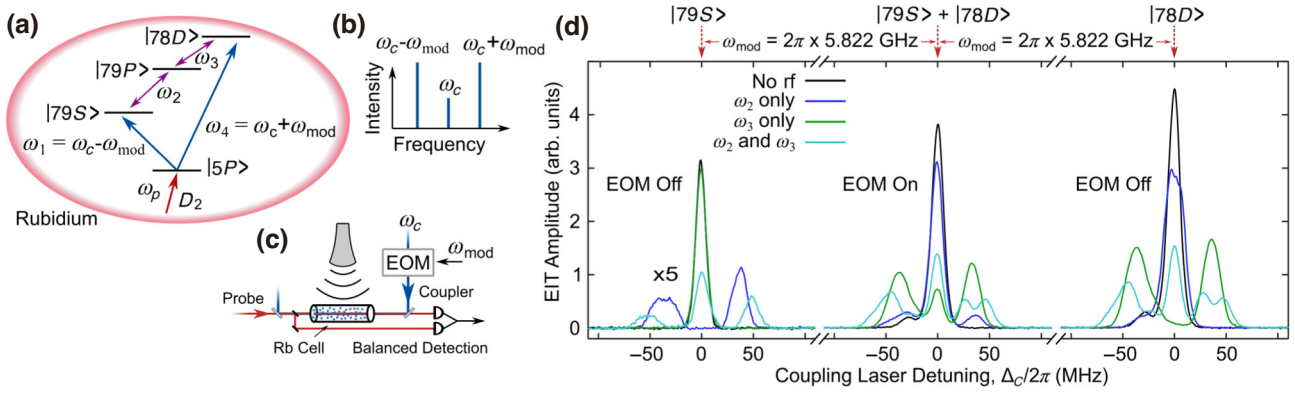


FIG. 1. Experimental details. (a),(b) A schematic of (a) the EIT ladder and Rydberg states used for the quantum interference scheme, as well as (b) the phase-modulating electro-optic modulator (EOM) used for coupling-laser sideband generation. (c) A schematic of the experimental setup with counterpropagating probe and coupling beams. (d) The EIT spectra of the Rydberg states used, with the two rf fields turned on and off as indicated.

resolution necessary for modern digital-modulation schemes such as phase shift keying [19].

In this work, we demonstrate the general applicability of closed-loop schemes using Rydberg states for phase-sensitive field-sensing applications and show how they can directly produce LO-equivalent functionality. We implement a quantum interferometric loop scheme for rf sensing where we leverage the versatility of such an approach by using a loop where the four transitions are comprised of two optical and two nondegenerate rf frequencies. We show that this scheme provides full 360° phase resolution on both rf fields. Furthermore, we clearly demonstrate that a closed-loop scheme establishes an LO-free quantum coherent reference frequency and phase that can be exploited analogously to the LO used in established Rydberg-mixer measurements [5]. Using this quantum reference, we perform LO-free demodulation of a quadrature phase-shift keying (QPSK) equivalent four-phase state signal at a symbol rate of 800 Hz. We reveal that the sensitivity relative to a traditional LO-based Rydberg mixer is reduced by as little as a factor of 5 and we expect significantly improved sensitivity and bandwidth using optimally chosen states [20]. Although the present implementation still requires an auxiliary rf field, a notable feature of this scheme is the possibility of an rf-free all-optical implementation that closes the loop using phase-locked optical fields to measure an rf field.

## II. EXPERIMENTAL

A schematic of the closed-loop scheme used for our experiment is shown in Fig. 1(a). The loop is comprised of four fields, $E_i, i = 1, \ldots, 4$, each with corresponding frequencies $\omega_i$, Rabi frequencies $\Omega_i$, and phases $\phi_i$. The probe field on the $D_2$ transition first couples the $^{85}$Rb $5S_{1/2}$ ground state to the $5P_{3/2}$ state. An electro-optic modulator (EOM) driven by an external phase-stable signal at a frequency $\omega_{\text{mod}} = 2\pi \times 5.822$ GHz generates sidebands on the coupling field [Fig. 1(b)] at $\omega_1 = \omega_c - \omega_{\text{mod}}$ and $\omega_4 = \omega_c + \omega_{\text{mod}}$ that then couple to the $79S_{1/2}$ and $78D_{5/2}$ states, respectively. These states are then linked through the $79P_{3/2}$ state via two rf-frequency transitions at $\omega_2 = 2\pi \times 7.292$ GHz ($S$-$P$ transition) and $\omega_3 = 2\pi \times 4.352$ GHz ($D$-$P$ transition). The phases and frequencies of this loop-state arrangement are related by $\omega_1 + \omega_2 + \omega_3 = \omega_4$ and $\phi_1 + \phi_2 + \phi_3 = \phi_4$. Using the two EOM-generated sidebands [Fig. 1(b)], these relationships reduce to $\omega_2 + \omega_3 - 2\omega_{\text{mod}} = 0$ and $\phi_2 + \phi_3 - 2\phi_{\text{mod}} = 0$. One notable benefit of this scheme is that any frequency or phase noise and/or drift in the coupling laser cancels out, with the only remaining dependence being on our phase-locked rf fields. This set of states is chosen based on the narrow bandwidth of our EOM around 5.8 GHz but this approach is generally applicable and we have verified that it works for other closed-loop state manifolds.

Our setup uses the established electromagnetically induced transparency (EIT) ladder approach to excite and probe the high-lying Rydberg states [21]. A schematic of the experimental setup, consisting of counterpropagating coupling and probe lasers that are spatially overlapped in a rubidium vapor cell, is shown in Fig. 1(c) and the rf fields are broadcast onto the cell using a standard-gain horn antenna. The EIT-induced change in probe transmission is detected using balanced photodetection. The EOM is inserted into the coupling-beam path to generate sidebands on the coupling-laser frequency $\omega_c$, located at $\omega_1$ and $\omega_4$ as described above.

## III. RESULTS

We begin by examining the EIT spectra of our system of states. In Fig. 1(d), we show a set of spectra of the bare $79S$ and $78D$ states (left and right, respectively) with the EOM turned off, where the $79S$ state EIT amplitude

is approximately 5 times weaker than that of 78*D*. As we probe the bare states, we see Autler-Townes (AT) splitting when the rf fields corresponding to the adjacent transitions are turned on [$\omega_2$ for 79*S* and $\omega_3$ for 78*D*, in the left and right plots of Fig. 1(d), respectively], where we ensure that the Rabi frequencies are equivalent: $\Omega_2 = \Omega_3 = 2\pi \times 80$ MHz. In contrast, when only the nonadjacent rf fields are applied ($\omega_2$ for 79*S* and $\omega_3$ for 78*D*), there is little effect on the EIT spectra; though a limited effect on the 78*D* state is seen due to the nearby transition to $76F_{7/2}$. This nearby transition is also likely responsible for the asymmetry seen in the AT doublet. When both rf fields are applied, we see two key effects: the AT splitting increases further and the central EIT peak reappears. The reappearance of the EIT peak is due to a two-photon Raman transition that we have described previously [22], which here resonantly links the 79*S* and 78*D* states.

We set up our interferometric loop by turning on the EOM and setting the coupling-laser frequency halfway between the 79*S* and 78*D* states, i.e., the sidebands are on resonance with these transitions. As a result, the sideband-generated 79*S* and 78*D* EIT peaks are spectrally superimposed when no rf is applied in Fig. 1(d) (center). With applied $\omega_2$ or $\omega_3$ rf fields, the corresponding constituent 79*S* and 78*D* peaks undergo AT splitting and the other peak remains unchanged as a residual central EIT peak. This superposition peak is dominated by the significantly stronger contribution of the 78*D* transition. When both rf fields are applied—thus completing the interferometric loop—we see a superposition of the AT doublets from the 79*S* and 78*D* states, as well as a central EIT peak that is due to the two-photon Raman transition. It is this configuration with the superimposed AT doublets and the two-photon Raman peak that we will use to examine the effect of rf phase.

We begin our examination of the rf phase with the effect of the phase of $\omega_3$ ($\phi_3$). In Fig. 2(a), we show a false-color plot of the superposition EIT peak amplitude as $\phi_3$ is swept over 360°. Phase-dependent (vertical) line cuts taken from the central (blue circles) and side peaks (open black circles and squares), shown on the right, reveal a clear oscillation in the amplitude with a depth of around 20% and a periodicity of 360°. The error bars in the phase-dependent line cuts are calculated from the standard deviation of ten measurements taken in sequence and primarily reflect the noise of the probe laser, while larger variations arise from

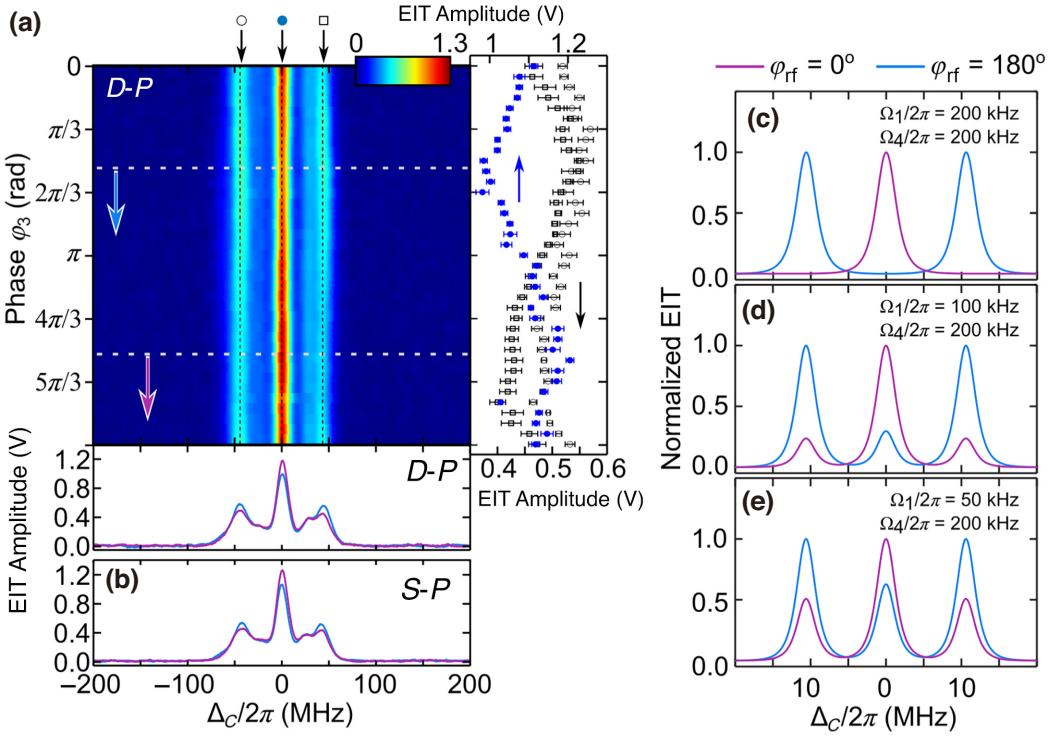


FIG. 2. Phase sensitivity. (a) A demonstration of the phase sensitivity on the *D-P* transition while the phase of the other field is held constant. The false-color plot shows the evolution of the EIT amplitude as a function of the corresponding rf phase ($\phi_3$). The right-hand panel shows the line cuts along each of the prominent EIT peaks as a function of the phase and the bottom panel shows the EIT spectra taken along the dashed lines in the false-color plot, indicated by the colored arrows. (b) Spectra showing the equivalent maxima in EIT amplitude as a function of the rf phase applied to the *S-P* transition ($\phi_2$). (c)–(e) Modeled results showing the evolution of the phase-modulation depth as a function of the difference in coupling-laser Rabi frequencies: (c) $\Omega_1/2\pi = 200$ kHz, $\Omega_4/2\pi = 200$ kHz; (d) $\Omega_1/2\pi = 100$ kHz, $\Omega_4/2\pi = 200$ kHz; (e) $\Omega_1/2\pi = 50$ kHz, $\Omega_4/2\pi = 200$ kHz.

fluctuations in our balanced detection due to thermal variations and drift. As confirmed in spectral (horizontal) line cuts taken along the white dashed lines and shown at the bottom, the central and AT-split side peaks oscillate out of phase.

Since the accumulated phase of our quantum interferometric loop is due to all fields involved, our measurement is sensitive to changes in phase of any of the fields. In Fig. 2(b), we show the response of the EIT signal to the phase of $\omega_2$ ($\phi_2$), where a comparable 20% modulation of the peak is also seen.

While our modulation depth is only around 20%, this is comparable to the relative amplitudes of the 79*S* and 78*D* EIT peaks that we are superimposing for our measurements. The optical field strengths of our EOM-generated sidebands are locked at the same value, so any differences in peak amplitudes are expected to be due to the transition dipole moments of the coupling-laser transitions. However, with transition dipole moments $\mu_4 \approx 2\mu_1$, we similarly expect a factor-of-2 difference in the EIT amplitudes. While we see EIT amplitudes differing by a factor of 2 for $n < 60$—in good agreement in our modeled EIT amplitudes—we see a large difference here for $n \approx 78$. The origin of this discrepancy is unclear but we expect that it relates to the increasingly higher density of nearby high-angular-momentum states at large $n$.

We theoretically investigate the effect of the optical Rabi frequencies $\Omega_1$ and $\Omega_4$ on the phase-dependent modulation depths. In Figs. 2(c)–2(e), we show the modeled [22,23] EIT amplitudes for in-phase and out-of-phase conditions, with $\Omega_1$ and $\Omega_4$ as indicated. Here, we see that a full modulation depth can be achieved if the Rabi frequencies—and thus the EIT amplitudes—of the two fields are the same, which decreases to 42% for $\Omega_1 = 4 \times \Omega_4$. We note that although quantitative changes in the modulation depth depend on the effective Rabi frequency, larger differences between $\Omega_1$ and $\Omega_4$ always lead to reduced contrast. These models also confirm the experimental observation noted above that the central and AT-doublet EIT peaks oscillate 180° out of phase as a function of the rf phase.

We now turn to the utility of our phase-sensitive quantum interferometric scheme. As noted above, the relative phases and frequencies of the three applied fields fix a reference frequency and phase on the fourth transition. For our measurements in Fig. 2(a), we use a frequency locked to that of this reference, which represents a homodyne measurement. We again emphasize that our reference phase and frequency are not the result of an applied field but, rather, are encoded in the quantum mechanical wave functions of the Rydberg states adjacent to our transition. This reference can then be used in a heterodyne configuration, analogously to a conventional Rydberg mixer [5].

In this approach, one of the rf fields, e.g., $\omega_3$, is applied at a detuned frequency $\omega_3' = \omega_3 + \delta$. This detuned frequency is equivalent to a resonant frequency with a time-varying phase, $\omega_3 + \delta = \omega_3 + d\phi/dt$, and the resulting oscillation in the EIT signal can be demodulated using lock-in detection at frequency $\delta$, where the lock-in phase provides a direct measure of the rf phase. For Figs. 3(a)–3(c), we detune and demodulate $\omega_3$, which can be used to measure either $\phi_2$ or $\phi_3$. In Fig. 3(a), we show the $\phi_2$-dependent in-phase ($I$) lock-in mixer signal as a function of $\Delta_C$, demonstrating the expected 360° phase sensitivity. The corresponding $\phi_2$-dependent evolution of the in-phase and out-of-phase (quadrature, $Q$) signals is shown in Fig. 3(b), taken along the spectral position of the dashed line in Fig. 3(a). We can clearly demodulate the $I$ and $Q$ components of the rf signal simultaneously, while the overall signal magnitude remains constant.

Next, we examine the dependence of our quantum interferometric Rydberg mixer on the electric field strength. In Fig. 3(c), we show the mixer magnitude as a function of $E_2$ at different values of $E_3$ as indicated. We can clearly see that for all values of $E_3$, there is a corresponding optimum value of $E_2$ that provides maximum sensitivity, where a weaker $E_2$ favors a weaker $E_3$ and vice versa. Since the signal magnitude remains monotonic over a large range of $E_2$, this approach can enable both phase and amplitude sensing.

We examine the low-field sensitivity of our approach in Fig. 3(d). Here, we use a lock-in-filter bandwidth of 1 Hz to measure the signal amplitude at low field strengths for normal Rydberg mixers applied on the *S*-*P* and *D*-*P* transitions individually [7], as well as our interferometric loop mixer probing the *S*-*P* and *D*-*P* resonant transitions. The normal Rydberg mixers are measured using an LO field and signal field sourced from two different signal generators to produce a beat note at 10 kHz, while the coupling-laser Rabi frequencies are identical to those in the loop measurements. In all cases, the LO or complementary-loop rf fields have been empirically optimized for low-field sensitivity. As we are measuring the magnitude ($R$) output of our lock-in, the noise floor is calculated based on the average of the measured data points below the sensitivity threshold for the *D*-*P* loop and used to determine the value for a signal-to-noise ratio (SNR) of 1. From this, we estimate sensitivities of approximately 0.15 mV/m $\sqrt{\text{Hz}}$ and 1 mV/m $\sqrt{\text{Hz}}$ for the *D*-*P* and *S*-*P* mixers, respectively, and sensitivities of 2 mV/m $\sqrt{\text{Hz}}$ and 6 mV/m $\sqrt{\text{Hz}}$ for the *D*-*P* and *S*-*P* interferometric loop mixers, respectively.

To demonstrate the general utility of our quantum interferometric loop Rydberg mixer, we broadcast a four-phase-state $\phi_3$ signal onto the atoms, generated using an IQ mixer to simulate a QPSK signal. In Fig. 4(a), we show the lock-in output of our simulated QPSK signal with a symbol rate of 800 Hz, showing the phase (black dots) together with the corresponding orthogonal $I$ and $Q$ channels (green and blue, respectively). The received constellation diagram in Fig. 4(b) shows the four well-resolved phase states

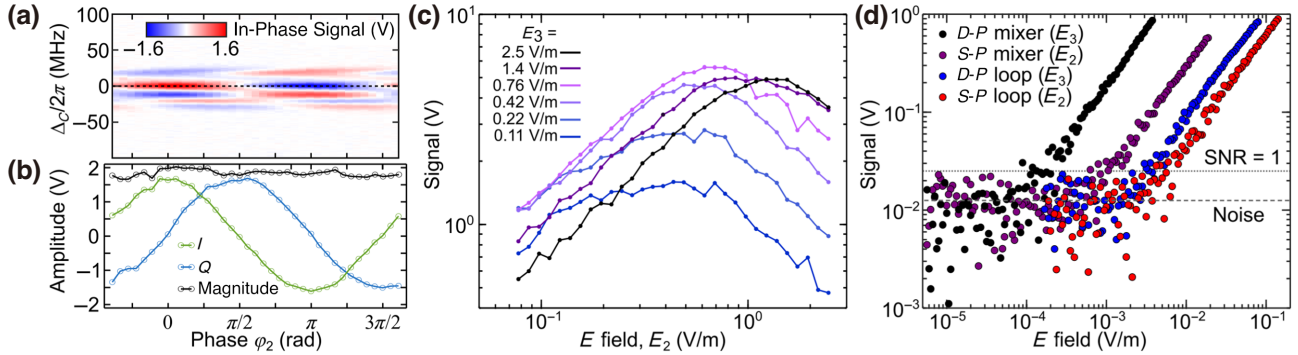


FIG. 3. The quantum interferometric Rydberg mixer. (a),(b) The in-phase ($I$) lock-in demodulated signal (a) as a function of $\phi_2$, together with (b) a line cut along the signal maximum along with the corresponding quadrature ($Q$) signal and the lock-in magnitude. (c) An $E$-field strength-dependent measurement shows a monotonic mixer sensitivity over a broad range. (d) Sensitivity measurements compare the field-dependent amplitudes of Rydberg mixers on the bare $D$-$P$ and $S$-$P$ transitions with sensitivities achieved using the quantum interferometric mixer on the $D$-$P$ and $S$-$P$ transitions independently.

detected using our scheme. We emphasize that our 800-Hz bandwidth was not bandwidth limited, but without the vector signal generator and analyzer used in previous work [12] it was chosen for illustrative purposes based on the instrumental and signal-level limitations of our approach.

## IV. DISCUSSION

The use of our phase-coherent quantum interferometric scheme offers notable advantages compared to conventional Rydberg-mixer approaches. First, due to the dependence of the signal on the accumulated phase over the interferometric loop, we can now detune one field to generate a mixer that measures the phase of a different field. With the necessary presence of at least four fields to complete the loop, this may enable new modulation and frequency-mixing schemes for the detection and demodulation of rf fields. The use of degenerate rf frequencies [19] is a special case of our approach. Using two degenerate transitions, the rf phase is accumulated on both transitions, $\phi_{\text{tot}} = \phi_2 + \phi_3 = 2\phi_{\text{rf}}$, where the doubled phase provides only 180° phase resolution and thus renders common phase-modulation schemes unusable. And although our present implementation does not do away with rf fields altogether, the ability to apply a field on one rf transition in order to measure another allows frequency separation of the two fields, potentially into distinct bands. This may be useful for sensing applications where broadcasting an LO field in the spectral vicinity of the signal of interest is undesirable. The capability to apply the LO at significantly higher frequencies than the signal field may also be beneficial in designing structures for resonant or evanescent LO coupling that are much smaller than the signal wavelength and thus only minimally perturb its propagation.

Our sensitivity measurements show a diminished sensitivity of our loop approach compared to standard Rydberg mixers on the same transitions. The $D$-$P$ interferometric loop mixer shows an order-of-magnitude decrease in sensitivity compared to the $D$-$P$ mixer, though it is only a factor of 5 less than the $S$-$P$ mixer. This underscores a key conclusion of Figs. 2(c)–2(e): the overall sensitivity of this approach is maximized when $\Omega_1 = \Omega_4$, i.e., the EIT amplitudes are the same, and we see that it is ultimately limited by the weaker of the two. As such, we expect that high sensitivity could nevertheless be achieved with our approach given a better-matched state manifold. Although the $nD$-$(n-1)F$-$(n+1)D$ state manifold provides better-matched and large transition dipole moments, we have found that the transitions connecting the $nD$-$(n+2)P$-$(n+1)D$ states are within a few hundreds of megahertz of the $D$-$F$ ones and thus adversely affect the sensitivity of the associated loop. We do expect improvement in Cs, however, where the $D$-$P$-$D$ transitions are well isolated.

Our overall mixer sensitivity is also reduced by a factor of around 20 relative to the record values reported in the literature [6,24]. The $E$-field sensitivity is a trade-off between high rf transition dipole moments at high $n$ and better state isolation and higher coupling-laser transition dipole moments at low $n$. Thus, it is not surprising that these high sensitivity values are achieved using higher-angular-momentum states but they also rely on lower principal quantum numbers in the vicinity of $n \approx 50$. As such, we would expect dramatic improvement using an EOM with higher operating frequency. In this context, it is important to note that although the origin of the discrepancy between our measured $S$- and $D$-state EIT amplitudes and those predicted by our model is unclear, this further underscores the benefit of operating at lower values of $n$, where this discrepancy disappears and smaller EIT ratios are seen. Concluding that the overall sensitivity of our quantum interferometric scheme can approach that of a traditional LO-based mixer, it is also clear that the

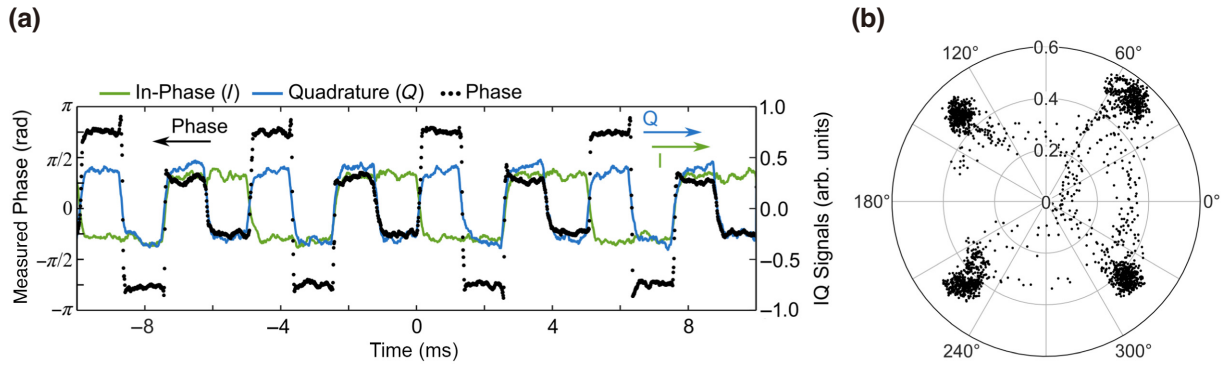


FIG. 4. Signal demodulation. (a) The phase plot, showing detection of a four-phase-state signal using the quantum phase mixer, along with the corresponding $I$ and $Q$ signals, at a symbol rate of 800 Hz. (b) The corresponding constellation diagram, showing the well-resolved phase states.

sensitivity improvements afforded by an LO-based approach also apply here.

Although we have used a four-photon scheme involving two optical and two rf fields, our demonstration of weak-field sensitivity suggests that it should be possible to replace one of the rf fields with an additional optical one—the Rabi frequencies of which are typically low—to enable all-optical Rydberg-atom $E$-field sensing. Elimination of the need for an external rf field altogether is attractive for angle-of-arrival measurements where a phase-front (propagation-direction) mismatch between the external field and the signal of interest will cause a reduced signal amplitude and phase accuracy. The inherent challenges of phase locking three optical fields to obtain a phase-stable loop can be achieved by several possible means. While potentially difficult to achieve, parametric generation generates phase-locked fields that will cancel any phase noise in the pump field through the loop, while phase locking using a frequency comb requires three separate lasers but may allow for a broader range of frequencies.

To illustrate the clear path forward toward all-optical rf phase detection using closed-loop quantum interferometric schemes, we lay out the framework for several possible schemes that we are currently implementing. These schemes are depicted in Fig. 5. The first scheme, shown in Fig. 5(a), is a three-optical-photon scheme where one ultraviolet (UV) laser is used to close the loop in a conventional two-photon cesium ($^{133}$Cs) scheme. In this case, the UV (319-nm) laser allows for a direct Rydberg excitation and an infrared (850-nm) and visible (510-nm) laser allow for another Rydberg excitation pathway with readout on the 850-nm laser. The applied rf field closes the loop for these two pathways and allows for a phase measurement of the rf field.

The second scheme, shown in Fig. 5(b), utilizes a six-wave-mixing approach similar to that presented in Ref. [25]. Here, the left-hand-side pathway uses two lasers (850 nm and 510 nm) to excite to a Rydberg state. In addition, a second pathway to a Rydberg state is achieved with a three-photon excitation scheme using 895-nm, 636-nm, and 2200-nm lasers. This three-optical-photon scheme is used for collinear $^{133}$Cs EIT schemes [26]. Here again, the applied rf field closes the loop and allows for a phase measurement of the rf field. In both of these schemes, by phase locking the set of independent lasers to a single stable frequency comb, we will be able to resolve the rf phase over 360°.

The last scheme, shown in Fig. 5(c), uses a single ground-state transition in Rb akin to the experimental study presented in this work. The loop is then completed

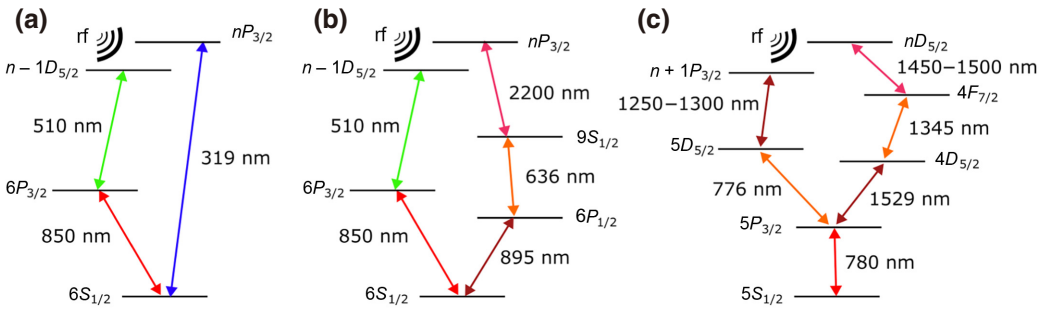


FIG. 5. All-optical excitation-loop schemes. Two possible all-optical phase-sensitive schemes in cesium using (a) three lasers and (b) five lasers, as well as (c) a rubidium scheme using a single ground-state transition.

with five optical fields to sense the single rf field. The optical fields used in this scheme provides low residual wave-vector mismatch and thus optimal line widths. All of the presented schemes provide full independent control of the strength of all fields in the loop and we can adjust the relative powers of the lasers on each side of the loop to balance the two sides in order to optimize the signal contrast with the rf phase. We have acquired all the lasers for the two different schemes shown in Fig. 5 and we will present data for the two schemes in a future publication.

## V. CONCLUSIONS

We have demonstrated a Rydberg-atom-based rf electric field sensor scheme that uses quantum interference over a closed loop of atomic transitions, with the phase and frequency fixed by the fields used. This approach provides full 360° phase-resolved field sensing without an applied local oscillator near the detected frequency. We further show that this approach enables LO-free functionality analogous to that of a traditional LO-based Rydberg mixer, where we demonstrate phase-resolved demodulation of a four-phase-state QPSK signal using our quantum interferometric mixer. These experiments demonstrate the clear-cut advantages of closed-loop quantum interferometric schemes for Rydberg-atom-based rf field sensing and, further, hopefully offer the potential for all-optical field sensing. Finally, with an eye toward developing these all-optical interferometric loops, we have described several schemes for LO-free all-optical rf phase detection.

## ACKNOWLEDGMENTS

This research was developed with funding from the Defense Advanced Research Projects Agency (DARPA).

The views, opinions, and/or findings expressed are those of the authors and should not be interpreted as representing the official views or policies of the Department of Defense or the U.S. Government. This paper is a contribution of the U.S. Government, not subject to U.S. copyright.

[1] A. Artusio-Glimpse, M. T. Simons, N. Prajapati, and C. L. Holloway, Modern rf measurements with hot atoms: A technology review of Rydberg atom-based radio frequency field sensors, IEEE Microw. Mag. **23**, 44 (2022).

[2] J. A. Sedlacek, A. Schwettman, H. Kübler, R. Löw, T. Pfau, and J. P. Shaffer, Microwave electrometry with Rydberg atoms in a vapour cell using bright atomic resonances, Nat. Photonics **8**, 819 (2012).

[3] H. Fan, S. Kumar, J. Sedlacek, H. Kübler, S. Karimkashi, and J. P. Shaffer, Atom based RF electric field sensing, J. Phys. B: At. Mol. Opt. Phys **48**, 202001 (2015).

[4] K. C. Cox, D. H. Meyer, F. K. Fatemi, and P. D. Kunz, Quantum-limited atomic receiver in the electrically small regime, Phys. Rev. Lett. **121**, 110502 (2018).

[5] M. T. Simons, A. H. Haddab, J. A. Gordon, and C. L. Holloway, A Rydberg atom-based mixer: Measuring the phase of a radio frequency wave, Appl. Phys. Lett. **114**, 114101 (2019).

[6] M. Jing, Y. Hu, J. Ma, H. Zhang, L. Zhang, L. Xiao, and S. Jia, Atomic superheterodyne receiver based on microwave-dressed Rydberg spectroscopy, Nat. Phys. **16**, 911 (2020).

[7] J. A. Gordon, M. T. Simons, A. H. Haddab, and C. L. Holloway, Weak electric-field detection with sub-1 Hz resolution at radio frequencies using a Rydberg atom-based mixer, AIP Adv. **9**, 045030 (2019).

[8] D. H. Meyer, P. D. Kunz, and K. C. Cox, Waveguide-coupled Rydberg spectrum analyzer from 0 to 20 GHz, Phys. Rev. Appl. **15**, 014053 (2021).

[9] X.-H. Liu, K.-Y. Liao, Z.-X. Zhang, H.-T. Tu, W. Bian, Z.-Q. Li, S.-Y. Zheng, H.-H. Li, W. Huang, H. Yan, and S.-L. Zhu, Continuous-frequency microwave heterodyne detection in an atomic vapor cell, Phys. Rev. Appl. **18**, 054003 (2022).

[10] D. H. Meyer, K. C. Cox, F. K. Fatemi, and P. D. Kunz, Digital communication with Rydberg atoms and amplitude-modulated microwave fields, Appl. Phys. Lett. **112**, 211108 (2018).

[11] A. K. Robinson, N. Prajapati, D. Senic, M. T. Simons, and C. L. Holloway, Determining the angle-of-arrival of a radio-frequency source with a Rydberg atom-based sensor, Appl. Phys. Lett. **118**, 114001 (2021).

[12] C. L. Holloway, M. T. Simons, J. A. Gordon, and D. Novotny, Detecting and receiving phase-modulated signals with a Rydberg atom-based receiver, IEEE Antennas Wirel. Propag. Lett. **18**, 1853 (2019).

[13] G. Morigi, S. Franke-Arnold, and G.-L. Oppo, Phase-dependent interaction in a four-level atomic configuration, Phys. Rev. A **66**, 053409 (2002).

[14] D. Shylla, E. Ogaro, and K. Pendey, Highly sensitive atomic based MW interferometry, Sci. Rep. **8**, 8692 (2018).

[15] A. F. Huss, R. Lammegger, C. Neureiter, E. A. Korsunsky, and L. Windholz, Phase correlation of laser waves with arbitrary frequency spacing, Phys. Rev. Lett. **93**, 223601 (2004).

[16] S. Kajari-Schröder, G. Morigi, S. Franke-Arnold, and G.-L. Oppo, Phase-dependent light propagation in atomic vapors, Phys. Rev. A **75**, 013816 (2007).

[17] J. Han, T. Vogt, C. Gross, D. Jaksch, M. Kiffner, and W. Li, Coherent microwave-to-optical conversion via six-wave mixing in Rydberg atoms, Phys. Rev. Lett. **120**, 093201 (2018).

[18] A. Kumar, A. Suleymanzade, M. Stone, L. Taneya, A. Anferov, D. I. Schuster, and J. Simon, Quantum-enabled millimetre wave to optical transduction using neutral atoms, Nature **615**, 614 (2023).

[19] D. A. Anderson, R. E. Sapiro, L. F. Gonçalves, R. Cardman, and G. Raithel, Optical radio-frequency phase measurement with an internal-state Rydberg atom interferometer, Phys. Rev. Appl. **17**, 044020 (2022).

[20] A. Chopinaud and J. D. Pritchard, Optimal state choice for Rydberg-atom microwave sensors, Phys. Rev. Appl. **16**, 024008 (2021).

[21] A. K. Mohapatra, M. G. Bason, B. Butscher, K. J. Weatherill, and C. S. Adams, A giant electro-optic effect using polarizable dark states, Nat. Phys. **4**, 890 (2008).

[22] S. Berweger, N. Prajapati, A. B. Artusio-Glimpse, A. P. Rotunno, R. Brown, C. L. Holloway, M. T. Simons, E. Imhof, S. R. Jefferts, B. N. Kayim, M. A. Viray, R. Wyllie, B. C. Sawyer, and T. G. Walker, Rydberg-state engineering: Investigations of tuning schemes for continuous frequency sensing, Phys. Rev. Appl. **19**, 044049 (2023).

[23] C. L. Holloway, M. T. Simons, J. A. Gordon, A. Dienstfrey, D. A. Anderson, and G. Raithel, Electric field metrology for SI traceability: Systematic measurement uncertainties in electromagnetically induced transparency in atomic vapor, J. Appl. Phys. **121**, 233106 (2017).

[24] N. Prajapati, A. K. Robinson, S. Berweger, M. T. Simons, A. B. Artusio-Glimpse, and C. L. Holloway, Enhancement of electromagnetically induced transparency based Rydberg-atom electrometry through population repumping, Appl. Phys. Lett. **119**, 214001 (2021).

[25] S. Borówka, U. Pylypenko, M. Mazelanik, and M. Parniak, Continuous wideband microwave-to-optical converter based on room-temperature Rydberg atoms, ArXiv:2302.08380 (2023).

[26] N. Prajapati, N. Bhusal, A. P. Rotunno, S. Berweger, M. T. Simons, A. B. Artusio-Glimpse, Y. Ju Wang, E. Bottomley, H. Fan, and C. L. Holloway, Sensitivity comparison of two-photon vs three-photon Rydberg electrometry, J. Appl. Phys. **134**, 023101 (2023).